Catalysis Today 138 (2008) 38–42

Contents lists available at ScienceDirect

Catalysis Today

journal homepage: www.elsevier.com/locate/cattod

Metal oxides nanoparticles on SBA-15: Efficient catalyst for methane combustion

G. Laugel [a,*], J. Arichi [a], M. Molière [b], A. Kiennemann [a], F. Garin [a], B. Louis [a]

[a] Laboratoire des Matériaux, Surfaces et Procédés pour la Catalyse, UMR 7515 du CNRS, 25 Rue Becquerel, 67087 Strasbourg, France
[b] GE Energy Products-Europe (GEEPE), 20 Avenue du Maréchal Juin, 9007 Belfort Cedex, France

ARTICLE INFO

Article history:
Available online 16 June 2008

Keywords:
Safety detector
Methane combustion
SBA-15
Co_3O_4
Mn_3O_4
Nanoparticles

ABSTRACT

Catalysts based on crystalline nanoparticles of Mn and Co metal oxides supported on mesoporous silica SBA-15 have been developed. These materials were characterized by XRD, BET and transmission electron microscopy (TEM) techniques. SBA-15 mesoporous silica was synthesized by a conventional sol–gel method using a tri-block copolymer as surfactant. Supported Mn_3O_4 and Co_3O_4 nanoparticles were obtained after calcination of as-impregnated SBA-15 by a metal salt precursor. The catalytic activity was evaluated in the combustion of methane at low concentration.

Co_3O_4/SBA-15 (7 wt.%) exhibits the highest performance among the different oxides. Furthermore, this novel generation of catalysts appeared as active as conventional $LaCoO_3$ perovskite, usually taken as reference for this reaction. Thanks to its organized meso-structures, SBA-15 material creates peculiar diffusion conditions for reactants and/or products.

1. Introduction

The detection of explosive gases and vapors is a critical safety function in industrial combustion processes [1–3]. Recent safety recommendations have implemented a detection limit of explosive gases corresponding to 5% lower explosive limit (LEL) for methane in the case of gas turbine industrial installations. While catalytic combustion is the method of choice for such detection, it becomes necessary to find efficient catalysts for methane complete oxidation at relatively low concentration and, for safety reasons, temperature (below 600 °C). Pd-based catalysts are usually considered as the most active for catalytic combustion of methane [1,4,5] and the most able to meet these safety constraints, however metal oxides M_yO_x (M=Mn or Co) and mixed metal oxides, i.e. perovskites [6–8], pyrochlores [9], offer a valuable alternative to noble metals with both an improved thermal stability and lower cost.

Bulk metal oxides generally possess a poor specific surface area (SSA) which seriously hinders their efficiency as catalysts. A convenient way to overcome this drawback is either to coat metal oxide nanoparticles on a support, or to disperse them within a porous host having a high SSA. Due to their narrow pore size distribution, high SSA and large pore volume, mesoporous silica materials such as MCM-41 and SBA-15 are promising candidates as catalyst supports [10–18]. Thanks to its thicker walls (3–6 nm), SBA-15 exhibits a higher thermal and hydrothermal stability when compared to thinner-walled MCM-41 material [19]. In addition, the higher stability of SBA-15 material renders it more suitable as a support in catalytic processes where thermal treatments and repeated regeneration are frequently encountered. The synthesis of SBA-15 materials is usually performed using poly(alkylene oxide) tri-block copolymer as surfactant under strongly acidic conditions [20], and has attracted great attention in the field of catalysis [21–23]. Furthermore, SBA-15 (SSA = 600–1000 m^2/g) consists of a hexagonal array of uniform tubular channels with tunable pore diameter in the range of 5–30 nm, thus being significantly larger than those from MCM-41 [24]. SBA-15 is therefore one of the most attractive silica host-material for metal or metal oxide nanoparticles.

Operating conditions in the coating of a catalytic phase on a support (nature of precursor, concentration, temperature) strongly influence the structure of its active phase. The conventional procedures, widely used for the synthesis of supported oxides, are impregnation and ion exchange techniques. Recently a novel method, the so-called "two-solvent" technique has attracting a considerable interest [25,26]. Indeed, this method allows the preparation of highly dispersed metal oxide nanoparticles within the mesopores which are used as confinement nanoreactors. Generally, inorganic precursors are first introduced into the channels of the mesoporous host. Afterwards, the desired oxide is obtained via an appropriate thermal treatment.

The present study deals with the synthesis and characterisation of Co_3O_4 and Mn_3O_4 nanoparticles coated on SBA-15 silica support. The catalytic activity of these materials was tested in the

* Corresponding author. Tel.: +33 3 90 24 27 60; fax: +33 3 90 24 27 61.
E-mail address: glaugel@chimie.u-strasbg.fr (G. Laugel).

0920-5861/$ – see front matter © 2008 Elsevier B.V. All rights reserved.
doi:10.1016/j.cattod.2008.04.027

combustion of methane at low temperature. The catalytic performance of these materials was compared with perovskite materials, usually taken as reference for this reaction [27,28].

2. Experimental

2.1. Synthesis of SBA-15 materials

The synthesis of SBA-15 material was carried out according to the procedure of Zhao et al. [20]. First, poly(ethylene oxide) poly(propylene oxide) poly(ethylene oxide) ($EO_{20}PO_{70}EO_{20}$, pluronic P123, BASF) tri-block copolymer was dispersed in aqueous hydrochloric acid solution ($1 < pH < 2$) under vigorous stirring. After one hour, a clear solution was obtained indicating a complete dissolution of the surfactant. Tetraethyl orthosilicate (TEOS), used as silica source, was added drop wise to the solution at 40 °C under stirring. Gelation and ageing were carried out at 40 °C for 24 h, followed by heating at 100 °C for 72 h in a sealed Teflon flask. The solid was filtered, washed several times with distilled water and dried at room temperature. Finally, the tri-block copolymer template was removed by calcination in air at 500 °C (heating rate 2 °C/min) for 6 h.

2.2. Mn_3O_4/SBA-15 and Co_3O_4/SBA-15 preparation

The manganese oxide and cobalt oxide supported catalysts on SBA-15 (Mn_3O_4/SBA-15 and Co_3O_4/SBA-15) were prepared according to the "two-solvent" technique [25]. SBA-15 was first suspended in dry hexane, used as hydrophobic solvent. Then, a desired amount of metal nitrate (7 wt.% or 30 wt.%) was dissolved in distilled water, quantity corresponding to the pore volume of SBA-15 determined by N_2 sorption. This solution (hydrophilic solvent) containing metal precursors was added drop wise. The gel was allowed to age for 2 h under stirring. The solid was recovered by filtration and dried in air. The samples were finally calcined at 700 °C for 6 h (heating rate 2 °C/min) to obtain the desired metal oxides Mn_3O_4 and Co_3O_4 [25]. Co_3O_4 metal oxide was also supported on silica gel (Grace, US) for comparison, while using the same procedure.

$LaCoO_3$ perovskite was prepared according to the resin method from metallo-organic propionate precursors [29,30]. First, lanthanum and cobalt acetate salts were dissolved in boiling propionic acid. Afterwards, the two solutions were mixed and stirred for 1 h under reflux conditions. Propionic acid was then evaporated until formation of a resin which hardened upon cooling. This resin was calcined at 700 °C for 4 h (heating rate 3 °C/min) to obtain the desired perovskite crystalline phase.

2.3. Characterisation techniques

The low-angle powder X-ray diffraction measurements were carried out on a X'PERT MDP apparatus (Philips, Cu Kα radiation) in the theta–theta geometry and associated to a thin film optics, including programmable divergence slit (1/32°), parallel plate collimator, flat Ge monochromator and proportional Xe detector. The system was equipped with TK450 camera of Anton Paar, as sample holder.

Wide-angle X-ray diffraction patterns were recorded on a Brucker D8 Advance diffractometer, with a Ni detector side filtered Cu Kα radiation (1.5406 Å) over a 2θ range of 5–90° and a position sensitive detector using a step size of 0.016° and a step time of 7 s.

Nitrogen adsorption–desorption isotherms were measured on a Micromeritics ASAP using nitrogen as gas probe at −196 °C. Before measurement, the sample was outgassed at 300 °C overnight to desorb moisture from the surface. The pore size distribution was determined from the adsorption branch of the isotherm and the SSA values were calculated using the BET model.

Transmission electron microscopy (TEM) measurements were performed on TOPCOM EM 002B microscope for high-magnification (Fig. 4a) and Hitashi S4800 FEG equipped with SE, YAG-BSE and TE detectors (Fig. 4b and c). The sample was dispersed in chloroform and deposited on a holey carbon film supported on Cu grid. EDX spectra were acquired to determine an average of the deposited metal oxides contained in the samples. The EDX spectra were acquired using 20 kV primary electron energy. Quantification was done using the standard-less ZAF correction method in the Genesis software from EDAX.

2.4. Catalytic tests

The catalytic combustion of methane was performed under air in a fixed-bed reactor under atmospheric pressure. The reactor is constituted by a U-shaped quartz tube of 5 mm of inner diameter. The catalyst (150 mg) was packed between quartz wool plugs and placed in the central part of the reactor. The void part of the reactor was filled by inert quartz pellets. The total gas flow of methane and air was set to 3 l/h, regulated by means of mass flow controllers (MFC, Brooks 5850 TR series). The concentration of methane was set to 5% of its lower explosion limit, i.e. 2500 ppm. The composition of the gas flow at the outlet of the catalytic reactor was analysed on-line by means of a Quad 200 (Agilent Technologies). A TCD detector was used for the Quad 200 which is composed by three modules with the Porapack U (PPU), methylpolysiloxane (OV1) and molecular sieve 5 Å (MS5A) columns.

3. Results and discussion

3.1. Characterisations of Co_3O_4/SBA-15 and Mn_3O_4/SBA-15 catalysts

The structures of the as-synthesized Co_3O_4 and Mn_3O_4 in SBA-15 mesopores, 7% in weight have been first examined by powder XRD, and the profiles are depicted in Figs. 1 and 2. Fig. 1 shows the low-angle diffraction pattern which displays the presence of three well-resolved reflexions that can be indexed as (1 0 0), (1 1 0) and (2 0 0) diffractions, thus associated with the well-ordered *p6mm* hexagonal symmetry [20]. It is noteworthy that the SBA-15 still exhibits a high degree of mesoscopic organisation even after the impregnation of Co_3O_4 and Mn_3O_4 nanocrystals. Moreover, high-magnification TEM image (Fig. 4a) evidences the hexagonal arrangement of the porous network after Co_3O_4 impregnation.

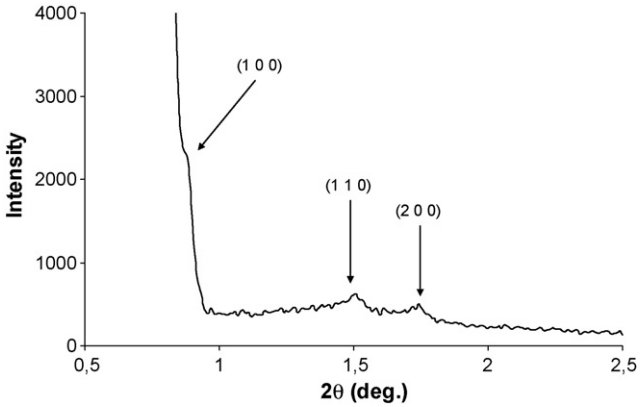

Fig. 1. Low-angle XRD pattern of the SBA-15 after cobalt oxide impregnation (7 wt.%).

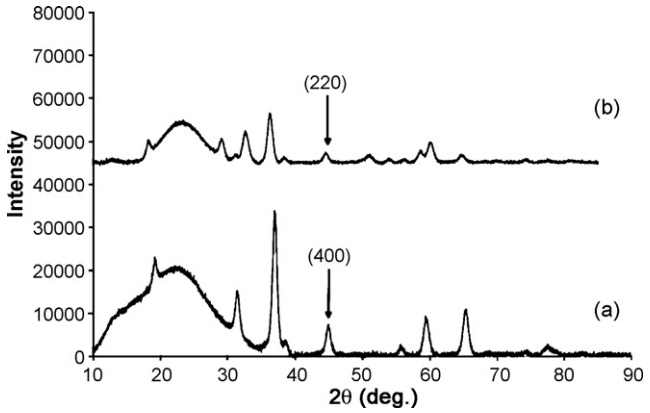

Fig. 2. XRD at wide angle of (a) Co_3O_4 nanoparticles and (b) Mn_3O_4 nanoparticles (7 wt.%).

Fig. 2a confirms the formation of crystallized Co_3O_4 cobalt oxide nanoparticles (JCPDS 43-1003). The broad peak between $10^\circ \leq 2\theta \leq 30^\circ$ corresponds to the mesoporous silica. The size of the nanoparticles was calculated as reported by Davidson and co-workers [26] using the Debye–Scherrer formula from the full width at half maximum (FWHM) of the (4 0 0) diffraction. A size of 11 ± 2 nm was estimated for Co_3O_4 nanoparticles. The indexation of the different reflections shown by the wide-angle diffraction pattern (Fig. 2b), clearly evidence the formation of a major Hausmannite Mn_3O_4 crystalline phase (JCPDS 080-0382) [31]. The particle size was calculated to be 10 ± 2 nm from the FWHM of the (2 2 0) diffraction peak of Mn_3O_4.

Results obtained by EDAX analysis of many samples confirmed the presence of metallic elements Mn and Co in the SBA-15 at desired loadings. An average content of metal of 6.7 wt.% and 7.2 wt.% was determined for Co_3O_4/SBA-15 (7 wt.%) and Mn_3O_4/SBA-15 (7 wt.%) samples, respectively. Again, the efficiency of the two-solvent method is confirmed for the coating of nanoparticles having both controlled size and loading.

The nitrogen adsorption–desorption isotherms of bare SBA-15 and Co_3O_4/SBA-15 are displayed in Fig. 3. The isotherm of siliceous SBA-15 (Fig. 3a) exhibits a type IV isotherm with H1 hysteresis following the IUPAC classification [32]. This profile is characteristic of mesoporous materials with one-dimensional cylindrical channels. A sharp inflection in the relative pressure (P/P_0) between 0.6 and 0.8 corresponds to capillary condensation within uniform mesopores and is a function of the pore diameter. The uniform pore size distribution is demonstrated by the sharpness of this step. The isotherm of the Co_3O_4/SBA-15 sample (Fig. 3b) also shows the typical profile of pristine SBA-15. However, the sharp inflection shifts toward lower relative pressures, suggesting that Co_3O_4 nanoparticles are present within SBA-15 mesopores. Indeed, both the pore diameter and the SSA were decreased from 6.8 nm to 5.6 nm, and from 785 m^2/g to 338 m^2/g for pristine SBA-15 and Co_3O_4/SBA-15, respectively. It is important to note that the mesoporous structure was preserved after catalytic runs.

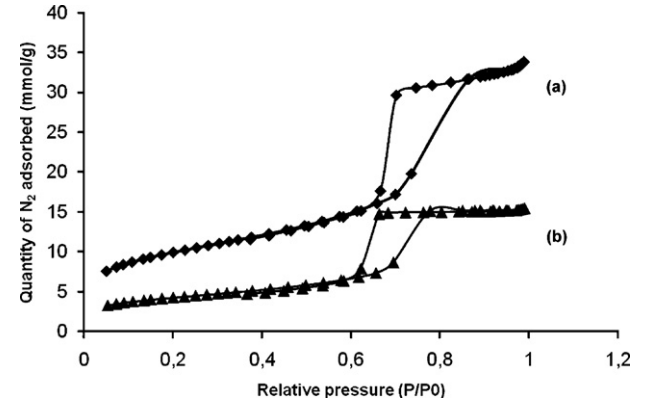

Fig. 3. Nitrogen adsorption–desorption isotherms of (a) SBA-15 and (b) Co_3O_4/SBA-15 (7 wt.%).

Mn_3O_4/SBA-15 microstructure was further investigated by TEM (Fig. 4b and c). Obviously, SBA-15 with a lower quantity of manganese oxide (7 wt.%) shows a homogeneous and high dispersion of nanoparticles formed within mesoporous channels

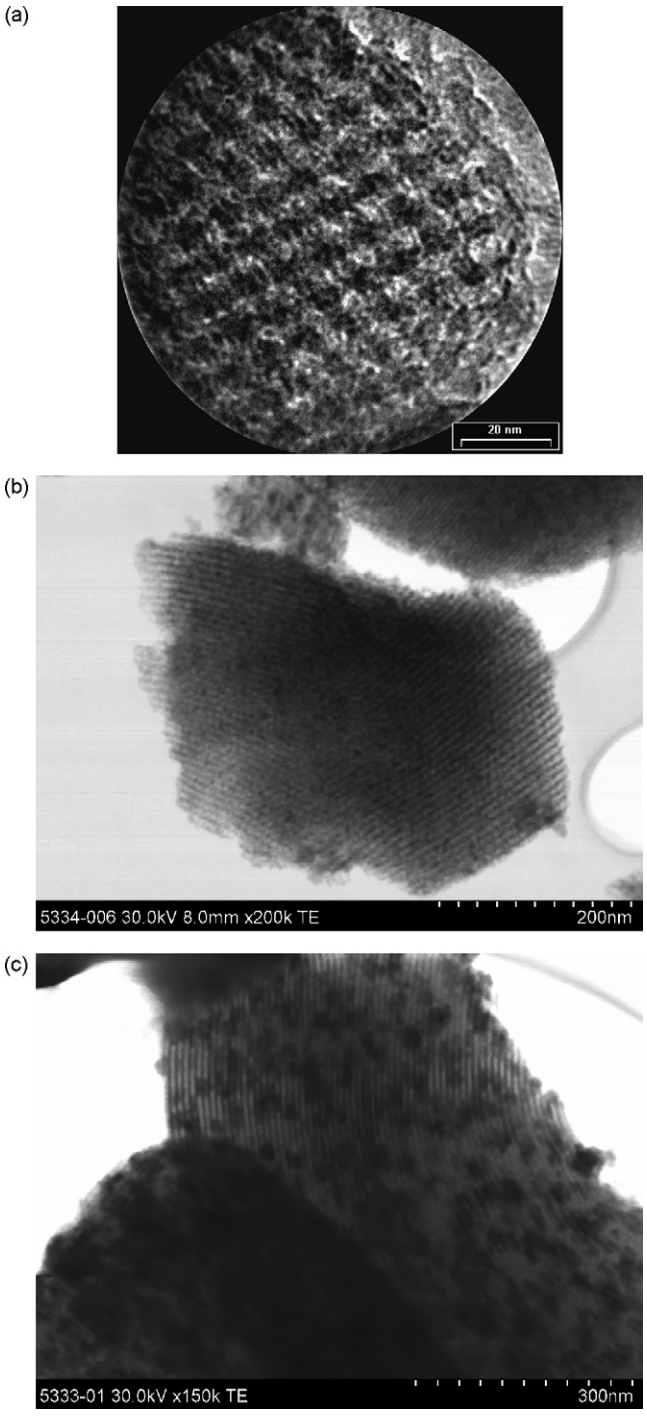

Fig. 4. TEM images of (a) Co_3O_4/SBA-15 (7 wt.%), (b) Mn_3O_4/SBA-15 (7 wt.%) and (c) Mn_3O_4/SBA-15 (30 wt.%).

Table 1
T_{50} and T_{90} temperatures for the different catalysts

	T_{50} temperature (°C)	T_{90} temperature (°C)
Co_3O_4/SBA-15 (7 wt.%)	506	576
Mn_3O_4/SBA-15 (7 wt.%)	534	588
Mn_3O_4/SBA-15 (30 wt.%)	552	615
Mn-Co/SBA-15 (7 wt.%)	541	589
$LaCoO_3$	514	591
Co_3O_4/SiO_2 (7 wt.%)	545	605

(Fig. 4b). In contrast, SBA-15 with a high manganese oxide loading (30 wt.%) presents larger aggregates (Fig. 4c). In spite of uncertainties in the size observed by TEM associated to changes in electron density [26], sizes of metal oxide nanoparticles (Mn_3O_4 and Co_3O_4) are consistent with the values calculated with Debye–Scherrer formula, i.e. 11 nm and 10 ± 2 nm for Co_3O_4 and Mn_3O_4, respectively.

3.2. Catalytic activity

Methane oxidation activity data are expressed in terms of CH_4 conversion with respect to the reaction temperature for the as-prepared manganese and cobalt oxides at different loadings supported on SBA-15. The temperatures of 50% (T_{50}) and 90% (T_{90}) of methane conversion were used to compare the activity of the catalysts (Table 1). Fig. 5 shows the dependence between CH_4 conversion with temperature for 7 wt.% and 30 wt.% supported manganese, 7 wt.% supported cobalt. For comparison, 7 wt.% of supported mixed equimolar manganese–cobalt was also tested (Fig. 5). It is clearly seen that a high loading of manganese oxide (30 wt.%), leads to a decrease in activity when compared to the 7-wt.% catalysts. The T_{50} temperature was reached 18 °C below for Mn_3O_4/SBA-15 (7 wt.%) than for the 30 wt.% material. This difference was further increased to 27 °C for T_{90} values (Table 1). According to the TEM images (Fig. 4b and c), the manganese oxide tends to form large aggregates at high loading (30 wt.%). Therefore a lower loading of active phase on SBA-15, can insure a homogeneous dispersion of nanoparticles within the channels of the mesoporous silica and thus allows an improved catalytic activity. Moreover, the activity of the Co_3O_4/SiO_2 (7 wt.%) catalyst in methane combustion is lower than the Co_3O_4/SBA-15 (7 wt.%) catalyst (Table 1). Thanks to its high SSA (SBA-15: 785 m^2/g and SiO_2: 300 m^2/g) and meso-structure, SBA-15 reach high dispersion of the Co_3O_4 nanoparticles.

Supported cobalt oxides on SBA-15 (7 wt.%) exhibit the highest catalytic activity in methane oxidation compared to the manganese oxide-based catalyst. These results are in line with those generally reported for total oxidation of hydrocarbons: Co_3O_4 > M-Mn_3O_4 > Cr_2O_3 > CuO [33–37]. However the difference in the T_{50} between Co_3O_4/SBA-15 and Mn_3O_4/SBA-15 is less pronounced at T_{90}, i.e. at high temperatures (≥570 °C). We can therefore suggest that the temperature of reaction strongly influences the behaviors of the two catalysts. Indeed, the mechanism of hydrocarbons combustion over metal oxide catalysts has long been discussed [38,39]. Generally, two different pathways are usually proposed for this reaction: (i) the Langmuir–Hinshelwood mechanism, where the reaction involves the adsorption of reactants on the catalyst surface and (ii) the Mars-van Krevelen mechanism, where the reactants are oxidized by lattice oxygen [40]. The latter usually occurs at elevated temperatures (>500 °C).

The Co_3O_4 crystalline phase is known to be a more efficient catalyst for methane oxidation at low temperature [41]. On the basis of the Langmuir–Hinshelwood mechanism, an optimal adsorption of methane at low temperature occurs at the surface of Co_3O_4 can explain its high activity compared to manganese oxide. However at high temperature conversion (500 °C), Mars-van Krevelen mechanism, becomes preponderant, thus a higher oxygen mobility in the manganese oxide lattice renders the catalytic activity of the two oxides in the same range [40].

An equimolar loading of Mn–Co (7 wt.%) on SBA-15 (Mn–Co/SBA-15) was prepared and also tested in the conversion of methane. From the light-off curves depicted in Fig. 5, the Mn–Co/SBA-15 catalyst behavior seems to exhibit the activity of a half equivalent of Mn_3O_4/SBA-15. Such inhibitor effect of supported bimetallic Co and Mn being less efficient than Mn/SBA-15 and Co/SBA-15 in terms of T_{50}, was already demonstrated by Li et al. [42] for the combustion of methane.

Perovskite type oxides (ABO_3) are particularly promising catalysts in the combustion of hydrocarbons owing to their high thermal stability and important oxygen mobility within the crystal lattice [8,43]. High catalytic activities in methane combustion over $LaBO_3$ (B═Co or Mn) were also reported by Arai et al. [6]. We have therefore performed comparison between bulk $LaCoO_3$ perovskite under the same conditions, i.e. 150 mg of catalyst and with the same catalyst bed length (mixture of $LaCoO_3$ with SiO_2). Fig. 6 shows a relatively same activity of Co_3O_4/SBA-15 compared to $LaCoO_3$. Furthermore, in case of Co_3O_4/SBA-15 (7 wt.%), the amount of active phase represents only 10.5 mg while, it constitutes 150 mg in case of bulk perovskite. Homogeneous

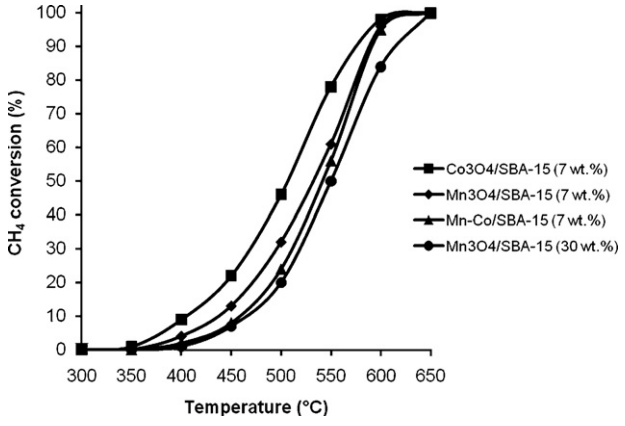

Fig. 5. Methane conversion as a function of temperature for manganese and cobalt oxides supported on SBA-15.

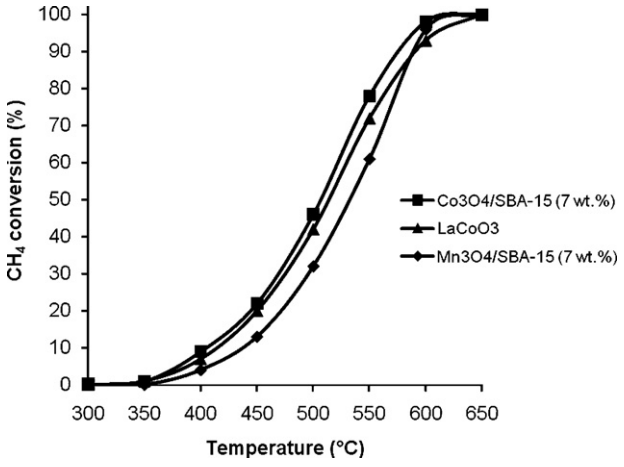

Fig. 6. Comparison between supported metal oxides on SBA-15 and $LaCoO_3$ perovskite.

dispersion of nanoparticles in the channels of the mesoporous SBA-15 provides a confined active site, able to adsorb and activate methane efficiently on different crystallite faces.

4. Conclusions

In summary, Mn_3O_4 and Co_3O_4 nanoparticles were highly dispersed on SBA-15 silica while using a two-solvent procedure, i.e. one hydrophilic, one hydrophobic. The synthesis procedure allowed a proper control of both the size and the loading of metal oxides.

Co_3O_4/SBA-15 (7 wt.%) exhibited the highest catalytic performance in the conversion of methane to carbon dioxide and water even at 5% of LEL concentration. This opens up a route to produce novel efficient combustion catalysts without Pd-use and at low metal loading.

Thanks to its mesoporous structure, SBA-15 seems to offer the appropriate pore architecture and size to ensure a high and homogeneous dispersion of Mn_3O_4 and Co_3O_4 oxides, thus creating a confinement media, being resistant to sintering.

Acknowledgements

The authors would like to thank GE Energy Products-Europe, for financial support (GL). Dr. B. Heinrich (GMO-IPCMS, France), G. Weinberg (FHI, Germany) and Y. Zimmermann (LMSPC, France) are gratefully acknowledged for technical assistance.

References

[1] P. Gelin, M. Primet, Appl. Catal. B 39 (2002) 1.
[2] M. Moliere, P. Cozzarin, S. Bouchet, P. Rech, in: Proceedings of the ASME Turbo 2005 Conference, Reno, June 6–9, 2005.
[3] M. Molière, P. Cozzarin, S. Bouchet, P. Rech, in: Proceedings of the ASME Turbo 2006 Conference, Barcelona, Spain, May 8–11, 2006.
[4] D. Ciuparu, M.R. Lyubovsky, E. Altman, L.D. Pfefferle, A. Datye, Catal. Rev. Sci. Eng. 44 (2002) 593.
[5] Y. Ozawa, Y. Tochihara, N. Mori, I. Yuri, J. Sato, K. Kagawa, Catal. Today 83 (2003) 247.
[6] H. Arai, T. Yamada, K. Eguchi, T. Seiyama, Appl. Catal. 26 (1986) 265.
[7] J.C. McCarty, H. Wise, Catal. Today 8 (1990) 231.
[8] M.A. Pena, J.L.G. Fierro, Chem. Rev. 101 (2001) 1981.
[9] J.M. Sohn, M.R. Kim, S.I. Woo, Catal. Today 83 (2003) 289.
[10] A. Corma, D. Kumar, Stud. Surf. Sci. Catal. 117 (1998) 201.
[11] Z. El Berrichi, L. Cherif, O. Orsen, J. Fraissard, J.P. Tessonnier, E. Vanhaecke, B. Louis, M.J. Ledoux, C. Pham-Huu, Appl. Catal. A 298 (2006) 194.
[12] Z. El Berrichi, B. Louis, J.P. Tessonnier, O. Ersen, L. Cherif, M.J. Ledoux, C. Pham-Huu, Appl. Catal. A 316 (2007) 219.
[13] B. Louis, C. Subrahmanyam, L. Kiwi-Minsker, B. Viswanathan, P.A. Buffat, A. Renken, Catal. Commun. 3 (2002) 159.
[14] Y.S. Ooi, R. Zakaria, A.R. Mohamed, S. Bhatia, Catal. Commun. 5 (2004) 441.
[15] E. Rivera-Muñoz, D. Lardizabal, G. Alonso, A. Aguilar, M.H. Siadati, R.R. Chianelli, Catal. Lett. 85 (2003) 147.
[16] A. Taguchi, F. Schuth, Micropor. Mesopor. Mater. 77 (2005) 1.
[17] A. Vinu, B.M. Devassy, S.B. Halligudi, W. Bohlmann, M. Hartmann, Appl. Catal. A 281 (2005) 207.
[18] L. Vradman, M.V. Landau, M. Herskowitz, V. Ezersky, M. Talianker, S. Nikitenko, Y. Koltypin, A. Gedanken, J. Catal. 213 (2003) 163.
[19] J. Jarupatrakorn, T.D. Tilley, J. Am. Chem. Soc. 124 (2002) 8380.
[20] D. Zhao, J. Feng, Q. Huo, N. Melosh, G.H. Fredrickson, B.F. Chmelka, G.D. Stucky, Science 279 (1998) 548.
[21] Y. Cao, J.-C. Hu, P. Yang, W.-L. Dai, K.-N. Fan, Chem. Commun. (2003) 908.
[22] V. Dufaud, M.E. Davis, J. Am. Chem. Soc. 125 (2003) 9403.
[23] V. Fornes, C. Lopez, H.H. Lopez, A. Martinez, Appl. Catal. A 249 (2003) 345.
[24] J.S. Beck, J.C. Vartuli, W.J. Roth, M.E. Leonowicz, C.T. Kresge, K.D. Schmitt, C.T.W. Chu, D.H. Olson, E.W. Sheppard, et al. J. Am. Chem. Soc. 114 (1992) 10834.
[25] M. Imperor-Clerc, D. Bazin, M.D. Appay, P. Beaunier, A. Davidson, Chem. Mater. 16 (2004) 1813.
[26] I. Lopes, N. ElHassan, H. Guerba, G. Wallez, A. Davidson, Chem. Mater. 18 (2006) 5826.
[27] M. Alifanti, J. Kirchnerova, B. Delmon, D. Klvana, Appl. Catal. A 262 (2004) 167.
[28] T.V. Choudhary, S. Banerjee, V.R. Choudhary, Appl. Catal. A 234 (2002) 1.
[29] G. Sinquin, C. Petit, J.P. Hindermann, A. Kiennemann, Catal. Today 70 (2001) 183.
[30] J.L. Rehspringer, J.C. Bernier, Mater. Rec. Soc. Symp. Proc. 72 (1986) 67.
[31] V. Escax, M. Imperor-Clerc, D. Bazin, A. Davidson, C.R. Chim. 8 (2005) 663.
[32] K.S.W. Sing, D.H. Everett, R.A.W. Haul, L. Mosenu, R.A. Pierotti, J. Rouquerol, T. Siemieniewska, Pure Appl. Chem. 57 (1985) 603.
[33] M. O'Connell, A.K. Norman, C.F. Huttermann, M.A. Morris, Catal. Today 47 (1999) 123.
[34] A. Torncrona, M. Skoglundh, P. Thormahlen, E. Fridell, E. Jobson, Appl. Catal. B 14 (1997) 131.
[35] Y.F. Yu Yao, J. Catal. 33 (1974) 108.
[36] Y.F. Yu Yao, J. Catal. 39 (1975) 104.
[37] M.F.M. Zwinkels, S.G. Järås, P.G. Menon, Catal. Rev. Sci. Eng. 35 (1993) 319.
[38] Y.F. Han, L. Chen, K. Ramesh, E. Widjaja, S. Chilukoti, I. Kesumawinata Surjami, J. Chen, J. Catal. 253 (2008) 261.
[39] L.D. Pfefferle, W.C. Pfefferle, Catal. Rev. 29 (1987) 219.
[40] Y.F. Han, K. Ramesh, L. Chen, E. Widjaja, S. Chilukoti, F. Chen, J. Phys. Chem. C 111 (2007) 2830.
[41] T.-C. Xiao, S.-F. Ji, H.-T. Wang, K.S. Coleman, M.L.H. Green, J. Mol. Catal. A 175 (2001) 111.
[42] W. Li, Y. Lin, Y. Zhang, Catal. Today 83 (2003) 239.
[43] L.G. Tejuca, J.L.G. Fierro, J.M.D. Tascon, Adv. Catal. 36 (1989).